PCCP

PAPER

View Article Online
View Journal | View Issue

Cite this: *Phys. Chem. Chem. Phys.*, 2022, **24**, 11967

Photoinduced reaction mechanisms in prototypical and bathy phytochromes†

María Fernández López,[a] Margarethe Dahl,[a] Francisco Velázquez Escobar,[a] Hernán Ruy Bonomi,[b] Anastasia Kraskov,[a] Norbert Michael,[a] Maria Andrea Mroginski,[a] Patrick Scheerer[c] and Peter Hildebrandt*[a]

Phytochromes, found in plants, fungi, and bacteria, exploit light as a source of information to control physiological processes *via* photoswitching between two states of different physiological activity, *i.e.* a red-absorbing Pr and a far-red-absorbing Pfr state. Depending on the relative stability in the dark, bacterial phytochromes are divided into prototypical and bathy phytochromes, where the stable state is Pr and Pfr, respectively. In this work we studied representatives of these groups (prototypical Agp1 and bathy Agp2 from *Agrobacterium fabrum*) together with the bathy-like phytochrome *Xcc*BphP from *Xanthomonas campestris* by resonance Raman and IR difference spectroscopy. In all three phytochromes, the photo-induced conversions display the same mechanistic pattern as reflected by the chromophore structures in the various intermediate states. We also observed in each case the secondary structure transition of the tongue, which is presumably crucial for the function of phytochrome. The three phytochromes differ in details of the chromophore conformation in the various intermediates and the energetic barrier of their respective decay reactions. The specific protein environment in the chromophore pocket, which is most likely the origin for these small differences, also controls the proton transfer processes concomitant to the photoconversions. These proton translocations, which are tightly coupled to the structural transition of the tongue, presumably proceed *via* the same mechanism along the Pr → Pfr conversion whereas the reverse Pfr → Pr photoconversion includes different proton transfer pathways. Finally, classification of phytochromes in prototypical and bathy (or bathy-like) phytochromes is discussed in terms of molecular structure and mechanistic properties.

Received 3rd January 2022,
Accepted 3rd May 2022

DOI: 10.1039/d2cp00020b

rsc.li/pccp

Introduction

Phytochromes control a variety of physiological processes in plants and prokaryotes.[1–5] These photoreceptors are composed of a photosensory core module (PCM) carrying a tetrapyrrole chromophore, and an output module that is activated or deactivated *via* light-induced structural changes in the PCM.[6,7] Thus, phytochromes act as photoswitches with two parent states, the red-absorbing Pr and the far-red absorbing Pfr state in which the chromophore adopts a *ZZZssa* and *ZZEssa* configuration, respectively (Fig. 1).[1]

The interconversion between Pr and Pfr is not exclusively light-induced. There is also a thermal reaction pathway (dark reversion) that leads to the respective parent state.[8–13] The ratio of the reaction rates from Pfr → Pr and from Pr → Pfr define the thermal equilibrium between the parent states, which in plant phytochromes and prototypical bacteriophytochromes is entirely on the Pr side.[16] Only in a sub-group of bacterial phytochromes, the so-called bathy phytochromes, the order of stability is reversed such that Pfr is the stable dark state.[3,17]

Although the various phytochromes differ with respect to the chemical constitution of the chromophore, the module composition, and – comparing plant and prokaryotic phytochromes – the type of functionally relevant protein structural changes, they share a common general reaction scheme of the PCM.[1,18] The photoinduced structural changes start with a *Z*/*E* photoisomerization of the methine bridge between rings C and D (Fig. 1) that is followed by thermal relaxations of the chromophore structure and its immediate environment, an intramolecular proton translocation, and finally the secondary structure change of a peptide segment (tongue) in the PHY domain.[19] This seems to be a general mechanistic pattern in all

[a] *Technische Universität Berlin, Institut für Chemie, Sekr. PC14, Straße des 17. Juni 135, D-10623 Berlin, Germany. E-mail: hildebrandt@chem.tu-berlin.de*
[b] *Leloir Institute Foundation, IIBBA-CONICET, Av. Patricias Argentinas 435 (C1405BWE), Buenos Aires, Argentina*
[c] *Charité – Universitätsmedizin Berlin, corporate member of Freie Universität Berlin and Humboldt-Universität zu Berlin, Institute of Medical Physics and Biophysics, Group Protein X-ray Crystallography and Signal Transduction, Charitéplatz 1, D-10117 Berlin, Germany*

† Electronic supplementary information (ESI) available. See DOI: https://doi.org/10.1039/d2cp00020b

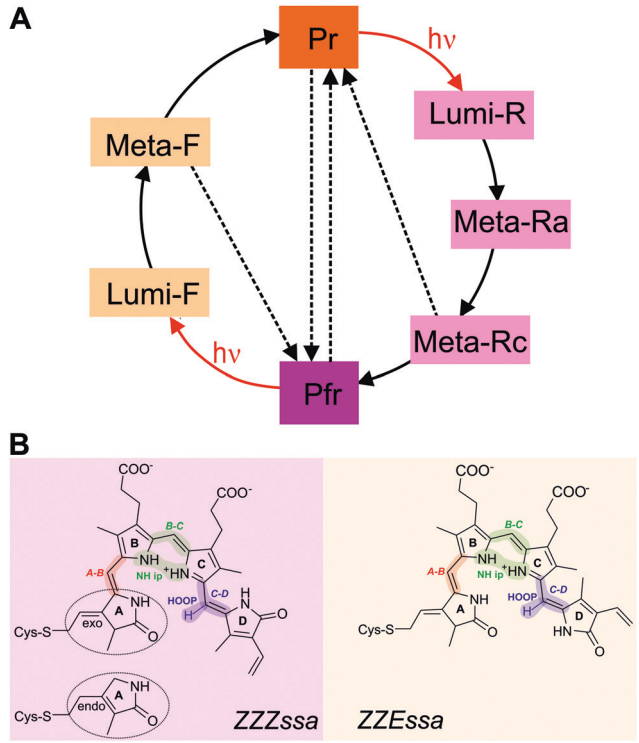

Fig. 1 (A) The general reaction scheme of phytochromes includes photochemical reactions (red arrows, *hν*), photoinduced thermal relaxation steps (black arrows), and pure thermal reactions (black dotted arrows).[8–13] States with *ZZZssa* and *ZZEssa* chromophore configurations (shown in B) are highlighted in (light-)orange and (light-)violet, respectively. The thermal transitions between the parent states Pr and Pfr (vertical arrows) define which of these states is the stable dark state, *i.e.* Pr in prototypical and Pfr in bathy phytochromes. (B) Structural formulas of the biliverdin chromophore in the *ZZZssa* (left) and *ZZEssa* (right) include a color code to illustrate the localization of important vibrational modes. The chromophore is attached to a Cys *via* ring A either in an exocyclic (Agp2) or endocyclic configuration (Agp1).[14,15]

phytochrome PCMs, regardless of the type of the tetrapyrrole chromophore, which is a phytochromobilin (PΦB), phycocyanobilin (PCB), and a biliverdin (BV) in plant, cyanobacterial, and bacterial phytochromes, respectively.[1,3,4] However, phototransformation pathways between the parent states may involve different proton transfer reactions. In prototypical phytochromes, Pr → Pfr phototransformation includes a proton transfer from the ring B or C N–H group of the chromophore to the solution phase during the formation of Meta-Rc.[20,21] Reprotonation takes place with the decay of Meta-Rc, concomitant to the structural transition of the tongue. In bathy phytochromes, the reverse phototransformation from Pfr to Pr is associated with the proton transfer from the propionic side chain of ring C (prop*C*) of BV to His278 (numbering refers to Agp2 from *Agrobacterium fabrum*) during the Meta-F to Pr transition, coupled to the restructuring of the tongue.[22–24] However, the mechanisms of the respective reverse reactions of bathy and prototypical phytochromes are not known.

In this work, we have carried out a comparative spectroscopic analysis of the Pr → Pfr and Pfr → Pr phototransformation pathways of three bacterial phytochromes. We employed resonance Raman (RR) spectroscopy to probe the chromophore structure in the various states of the photocycle.[25–30] We have chosen the Fourier-transform Raman technique which due to the near-infrared excitation (1064 nm) avoids unwanted photochemistry and fluorescence but still provides a sufficiently strong pre-resonance enhancement of the chromophore bands due to the energetic proximity with the first electronic transition.[29,30] RR spectroscopy was complemented by IR difference spectroscopy to determine protein and chromophore structural changes during the photoconversion.[31–35] The photoreceptors that were studied include representatives of prototypical and bathy phytochromes from *A. fabrum*, *i.e.* Agp1 and Agp2, respectively, and the bacterial phytochrome *Xcc*BphP from the plant pathogen *Xanthomonas campestris pv. Campestris*.[36] *Xcc*BphP, which regulates the infection of cruciferous plants,[37,38] was previously characterized as a bathy-like phytochrome since its dark reversion to Pfr is complete in the PCM alone but reaches "only" *ca.* 85% for the full-length protein.[36] Here, we determined common and distinct structural characteristics that are in part related to specific mechanistic properties. It was found that all phytochromes show the same Pr → Pfr photoconversion mechanism with the same proton transfer processes, whereas there are differences in the proton transfer pathways associated with the Pfr → Pr route in bathy phytochromes (Agp2) on the one hand and prototypical (Agp1) and the bathy-like phytochrome (*Xcc*BphP) on the other hand.

Materials and methods

Agp1 and Agp2 were expressed and purified as full-length and PCM variants as described previously.[9,15] *Xcc*BphP was generated as full-length protein according to the previously published procedure.[39] For vibrational spectroscopic experiments, the buffered solution of the purified protein was concentrated up to an optical density at 750 nm of *ca.* 40 using an Amicon centrifugal filter (MWCO 30 K, 15 800 g, 4 °C). H/D exchange was achieved by the same procedure but using a buffered solution in D_2O (pD 7.8). For the IR absorption measurements, the sample was incubated overnight in D_2O buffer, followed by another concentration/dilution cycle.[13] UV-vis absorption spectra in the Pr and Pfr state and the dark reversion kinetics were identical to those reported previously.[10,15,24,36]

Resonance Raman spectroscopy

RR measurements were performed using a Bruker Fourier-transform Raman spectrometer RFS 100/S with 1064 nm excitation (Nd-YAG cw laser, line width 1 cm^{-1}), equipped with a nitrogen-cooled cryostat from Resultec (Linkam). All spectra of the samples in frozen solution were recorded at *ca.* −190 °C with a laser power at the sample of 640 mW and an accumulation time of typically one hour. In order to identify potential laser-induced damage of the phytochrome samples, RR spectra before and after a series of measurements were compared. In no case changes between these control spectra were determined. Protein and buffer Raman bands were subtracted on

the basis of a Raman spectrum of apo-phytochrome. To generate the Pfr and Pr states, the sample was illuminated at ambient temperature for up to two minutes by a LED of 660 and 785 nm, respectively, followed by rapid cooling to *ca.* −190 °C to block thermal back reactions. This was particularly important for accumulating the Pr state of Agp2 due to the fast thermal Pr → Pfr back reaction at ambient temperature. Nevertheless, spectral contributions from Pfr could not be completely avoided. Intermediates of the respective photoconversion routes were then accumulated by irradiation of Pr (with 660 nm) or Pfr (with 785 nm) for two to five minutes at an irradiation temperature that was sufficiently low to block the decay of the desired intermediate. After photoconversion, the sample was cooled to −190 °C for the Raman measurement. Residual contributions from the unphotolysed state or unwanted decay products were removed by spectra subtraction using the OPUS software (Bruker). A more detailed description is given elsewhere.[9]

IR spectroscopy

IR spectroscopic measurements were carried out in the transmission mode at 20 °C using a Bruker Tensor 27 or IFS66v/s FTIR spectrometer.[24] Spectra were recorded with 200 single scans and a spectral resolution of 2 cm^{-1} and the double-sided acquisition mode. The Pr → Pfr conversion was achieved by continuous sample illumination with built-in diode arrays (780 and 670 nm). Difference spectra were obtained by subtraction of the initial state spectrum from the illuminated state spectrum.[24]

Results

We studied the RR and IR difference spectra of Agp1, Agp2, and *Xcc*BphP. Vibrational assignments based on isotopic labelling and theoretical calculations were discussed in detail previously.[9,22–24,40–42] These results as well as the data presented in this work allowed for a consistent band assignment in most cases. Here, we focused on those vibrational modes that provide information about specific structural properties and changes. These are particularly the modes in the region between 1500 and 1700 cm^{-1}, involving the stretching coordinates of the methine bridges (*cf.* Fig. 1). Further spectroscopic data are presented in the ESI.† The spectra were obtained from the full-length proteins unless noted otherwise. In general, differences between the full-length and PCM version mainly refer to the kinetics of the thermal conversion as discussed in detail previously.[11,22]

The Pfr state

The RR spectra of the Pfr state display the characteristic band pattern that is dominated by two strong bands originating from the C–D methine bridge, the C=C stretching (C–D) at *ca.* 1600 and the hydrogen-out-of-plane (HOOP) mode at *ca.* 810 cm^{-1} (Fig. 2 and Fig. S1, ESI†).[40] A careful inspection, however, reveals some important differences. Agp1 and *Xcc*BphP show a distinct shoulder at the high wavenumber side which is due to the A–B stretching mode with a small contribution from a mode including the C=C stretching of ring D and its vinyl substituent (ring D mode). More precisely, in Agp1 – as in all other prototypical phytochromes studied so far – there are two A–B stretching components which reflect a temperature-dependent equilibrium between two Pfr sub-states differing with respect to conformational details of the A–B methine bridge.[40,43] In Agp2, the A–B and ring D stretching modes are very weak and similar in frequency to the dominant C–D stretching such that they can only be identified by selective H/D substitution (Fig. S2, ESI†).[22] The heterogeneity of Agp1 also includes the C–D methine bridge, indicated by the low-frequency shoulder of the 809 cm^{-1} HOOP mode,[40] whereas in both *Xcc*BphP and Agp2 this band displays a largely symmetric lineshape. Also, the relatively weak bands of Agp1 at 853 and 842 cm^{-1} represent a characteristic feature of the structurally heterogeneous Pfr state. These two bands, found in all prototypical phytochromes, may be assigned to the N–H out-of-plane mode of rings A and B.[40] They are not observed in Agp2 and other bathy phytochromes,[40] whereas in *Xcc*BphP only the lower frequency component at 842 cm^{-1} is detected with considerable intensity.

The most striking spectral property of the Pfr states of classical bathy phytochromes such as Agp2, *Pa*BphP (*Pseudomonas aeruginosa*), and *Rp*BphP6 (*Rhodopseudomas palustris*), which clearly distinguishes them from prototypical phytochromes, refers to the strongly retarded H/D exchange at ring D (Fig. S2, ESI†).[22,23] Also in *Xcc*BphP, H/D exchange of all pyrrole ring N–H groups is only possible after a complete photocycle whereas in the Pfr state exchange of the ring D N–H group is drastically decelerated, presumably due to the strong interactions with the side chain of Asp199.[22,23] The second characteristic feature of bathy phytochromes is the protonated

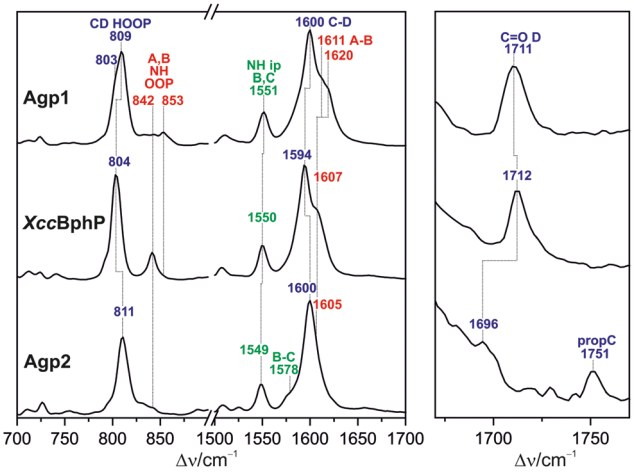

Fig. 2 RR spectra of the Pfr states of Agp1, *Xcc*BphP, and Agp2 (PCM) in the region of the torsional and HOOP modes and the C=C stretching region (left panel) and the C=O stretching region (right panel). The color code of the peak labels refers to Fig. 1, reflecting the localization of the modes to specific parts of the tetrapyrrole. The assignment of these modes is listed in Table 1.

prop*C* in Pfr, indicated by a band at 1750 cm^{-1} due to the prop*C* C=O stretching (Fig. 2).[22,23] The proton is released during the Meta-F → Pr transition (*vide infra*). A band at *ca.* 1750 cm^{-1} is missing in both *Xcc*BphP and Agp1 (Fig. 2). Also, the ring D C=O stretching is at similar positions in *Xcc*BphP (1712 cm^{-1}) and Agp1 (1711 cm^{-1}) but distinctly upshifted compared to Agp2 (1696 cm^{-1}) (*vide infra*).

Intermediates of the Pfr → Pr conversion

Lumi-F is the primary photoproduct of Pfr that can be cryogenically trapped.[24] The trapping range of Lumi-F is between −140 and −120 °C for all three phytochromes. This intermediate is expected to exhibit a distorted *ZZZssa* chromophore structure. As a consequence, normal mode compositions and frequencies are altered compared to the more relaxed chromophore geometries of Pfr or Pr, specifically as far as the modes are concerned that are localized at the isomerization site. For the relaxed *ZZEssa* configuration, the prominent C–D stretching at *ca.* 1600 cm^{-1} is predicted to be accompanied by a mode above 1630 cm^{-1} and with low intensity, that is localized in ring D and its vinyl substituent.[40] As shown by selective deuteration experiments for Agp2 and *Xcc*BphP, in Lumi-F the two modes mix such that they both include similar potential energy distributions and thus display comparable relative intensities (Fig. S2–S4, ESI†). Furthermore, both modes are closely spaced in frequency and distinctly upshifted compared to the C–D stretching mode of Pfr. Albeit not directly proven due to the lack of selective isotopic labelling, this scenario seems to hold also for the Lumi-F state of Agp1. As a consequence, the weakly Raman-active B–C stretching mode that undergoes only a small upshift upon Pfr → Lumi-F transition becomes now detectable at the low frequency side of the C–D stretching mode in all three phytochromes (Fig. 3). In Agp2 and *Xcc*BphP, the frequency upshifts of the A–B stretching modes are comparable or smaller than those of the respective C–D modes such that they are obscured by the bands of the latter modes in Lumi-F. Conversely, the A–B stretching modes are clearly detectable in the Lumi-F state of Agp1 due to the *ca.* 30 cm^{-1} upshift for both conformers. In Agp1, the structural heterogeneity is also reflected by the ring B/C N–H ip in-phase (RR-active) and out-of-phase (IR-active) modes.[30,40,44] The RR-active mode is usually observed at *ca.* 1550 and 1570 cm^{-1} in Pfr and Pr, respectively. In Lumi-F of Agp1, two bands are observed with one of them largely unchanged compared to Pfr (1551 cm^{-1}) whereas the other one is observed at a distinctly higher frequency (1569 cm^{-1}).

The subsequent thermal relaxation products Meta-F are stable in a wide temperature range between −120 and −30 °C in all three phytochromes. Here, the methine bridge stretching modes are distinctly upshifted by *ca.* 10 cm^{-1} (compared to Lumi-F) to the same or similar positions observed in the final product Pr (Fig. 3 and Fig. S5, S6, ESI†). Thus, also in *Xcc*BphP and Agp2, the A–B stretching modes are now clearly detectable. These relatively large shifts reflect the conformational relaxations of the chromophore in the binding pocket. As a result, a relaxed tetrapyrrole structure is stabilized that presumably does not differ significantly from that in Pr. One of the few characteristic spectral differences between Meta-F and Pr is the N–H ip of rings B and C which is found at *ca.* 1550 and 1570 cm^{-1} in Pfr and Pr, respectively.[24] In Meta-F it is observed at *ca.* 1560 cm^{-1} in Agp1 and *Xcc*BphP but at 1553 cm^{-1} in Agp2 (Fig. 3). Obviously,

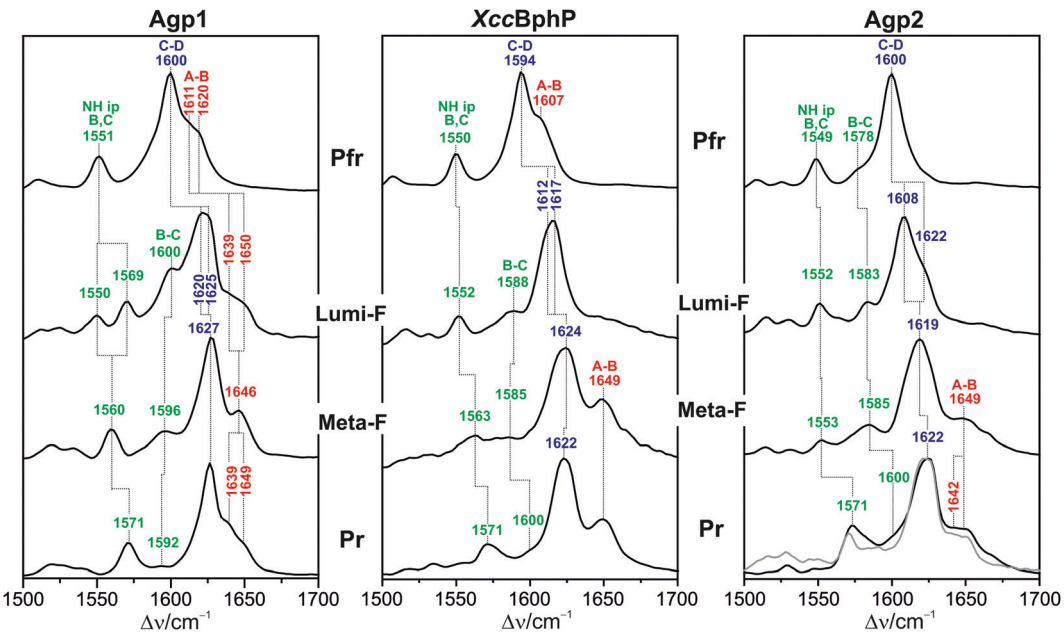

Fig. 3 RR spectra of the states of the Pfr → Pr photoconversion of Agp1 (left), *Xcc*BphP (middle), and Agp2 (right) in the C=C stretching region. The gray spectrum in the right panel (bottom) represents the pure keto tautomer of Pr of Agp2, obtained after subtracting the enol contribution.[22] The color code of the peak labels refers to Fig. 1, reflecting the localization of the modes to specific parts of the tetrapyrrole. The assignments of these modes are listed in Table 1.

the hydrogen bonding interactions of the ring B and C N–H group, that control the frequency of this mode,[45] are still similar to those of Pfr.

The main structural difference between the Pr states of the three phytochromes is the presence of an enol tautomer in Agp2.[22] Although a keto-enol tautomerism is most likely operative also for the dark reversion mechanism of all phytochromes,[46] only Agp2 displays an appreciable contribution of the enol tautomer that is even slightly higher in the full-length protein than in the PCM module (Fig. 3 and Fig. S6, ESI†).

Intermediates of the Pr → Pfr conversion

The photoinduced back reaction of Pr to Pfr is initiated by the $Z \rightarrow E$ isomerization of the C–D methine bridge. For prototypical phytochromes, including Agp1, the first intermediate Lumi-R was studied in detail previously.[9] The chromophore exhibits a highly distorted C–D methine bridge as indicated by the large 30 cm^{-1} downshift of the C–D stretching mode and the considerable RR activity of the HOOP modes (Fig. 4 and Fig. S7, ESI†). Also the geometry of the A–B methine bridge is altered, mirrored by the 20 cm^{-1} downshift of the A–B stretching mode. In Agp1, Lumi-R could be cryo-trapped in a wide temperature range from −140 to −80 °C,[9] whereas in Agp2 this intermediate was only stable until −120 °C. The shifts of the C=C stretching modes and the ring B/C N–H ip mode in Lumi-R of Agp2 were largely similar as in Agp1. The thermal decay of Lumi-R led to Meta-Ra which was stable up to −40 and −60 °C in Agp1 and Agp2, respectively.[9] Most surprisingly, the Meta-Ra state displays a RR spectrum very similar to that of Pr (Fig. 4 and Fig. S8, ESI†) in both Agp1 and Agp2. Only the C–D stretching mode is observed at a lower frequency than in Pr and in general the bands in the C=C stretching region appear to be broader. In contrast, Meta-Ra of Agp2 shows a C–D stretching mode at 1605 cm^{-1} that is even lower in frequency than that of Lumi-R (1609 cm^{-1}) and already close to that of Pfr (1600 cm^{-1}).

*Xcc*BphP displays a different behavior than Agp1 and Agp2 since the first intermediate that could be trapped required temperatures as high as −100 °C. Moreover, the spectrum of this intermediate is very similar to that of the Meta-Ra state of Agp1. Most likely, the thermal barrier for the transition from Lumi-R to Meta-Ra is very low in *Xcc*BphP such that an accumulation of Lumi-R is impaired.

A unique mechanistic property of the Pr → Pfr transformation of prototypical phytochromes is the transient deprotonation of ring B/C.[21,28,47] The deprotonated tetrapyrrole gives rise to a low extinction coefficient of the first electronic transition and thus leads to only weak resonance enhancement of the Raman bands upon excitation with 1064 nm. The RR spectrum of Meta-Rc is, therefore, the only spectrum, which includes notable contributions from Raman bands of the protein matrix (Fig. 5 and Fig. S9, ESI†).

The RR spectrum of the deprotonated tetrapyrrole chromophore lacks the N–H ip bending of rings B and C. In protonated species, this mode gives rise to a band between 1550 and 1575 cm^{-1} that shifts down to 1050–1070 cm^{-1} upon H/D

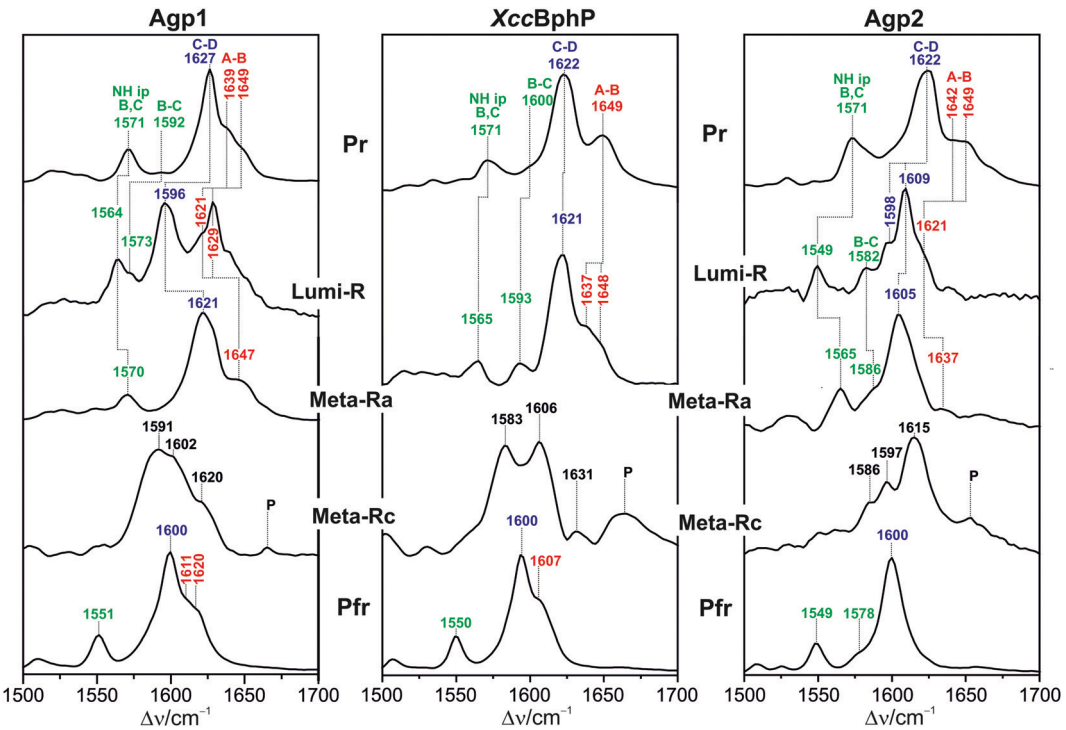

Fig. 4 RR spectra of the states of the Pr → Pfr photoconversion of Agp1 (left), *Xcc*BphP (middle), and Agp2 (right) in the C=C stretching region. The color code of the peak labels refers to Fig. 1, reflecting the localization of the modes to specific parts of the tetrapyrrole. The assignment of these modes is listed in Table 1. "P" denotes bands originating from the apoprotein.

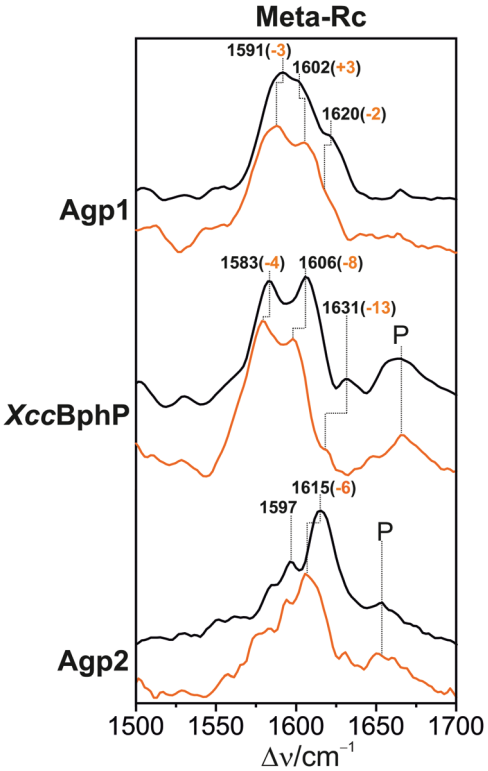

Fig. 5 RR spectra of the Meta-Rc states of Agp1, *Xcc*BphP, and Agp2 in the C=C stretching region. The black and orange traces correspond to the spectra measured in H_2O and D_2O, respectively. The assignments of the modes are listed in Table 1. "P" indicates Raman bands of the protein.

exchange. Furthermore, the C=C stretching region of deprotonated tetrapyrroles is characterized by two strong bands between 1580 and 1615 cm^{-1}, separated by *ca.* 10–20 cm^{-1} and displaying only small H/D isotopic shifts.[13,21] These criteria also hold for the intermediates of Agp2 and *Xcc*BphP trapped at −50 and −20 °C, respectively, and thus at similar temperatures as in Agp1 (−30 °C). Hence, we conclude that also Agp2 and *Xcc*BphP form a Meta-Rc intermediate with a deprotonated chromophore. The removal of a proton from one of the pyrrole nitrogens substantially alters the composition of the normal modes.[9,22–24,40–42,48–51] Furthermore, the vibrational band pattern appears to be similar for most of the tetrapyrroles and their various isomers.[48–51] Therefore, we assume that the differences in terms of relative intensities, frequencies, and H/D isotopic shifts in the spectra of the three Meta-Rc states reflect different protonation patterns.[51] In this respect, the prominent bands in the C=C stretching region from 1580 to 1650 cm^{-1} are particularly sensitive spectral markers. As shown for PCB, the frequency of the most intense band is predicted to be lower by *ca.* 15 cm^{-1} if ring C instead of ring B is deprotonated.[51] Furthermore, in the ring-C deprotonated tautomer this band is accompanied by a second band at higher frequency and similar intensity whereas its counterpart in the ring-B deprotonated tautomer displays a much weaker intensity. Assuming that these patterns also hold for BV (*vide supra*), we conclude that in the Meta-Rc state of Agp2 ring C should be preferentially protonated, whereas in *Xcc*BphP and presumably also in Agp1 the proton is expected to reside mainly on ring B.

Protein structural changes

Protein structural changes were probed by IR difference spectroscopy (Fig. 6). In the region of the amide I bands (1620–1680 cm^{-1}), which are diagnostic of the secondary structure of proteins, we note qualitatively the same changes in all three proteins. These changes can be largely attributed to restructuring of the tongue segment from a coil/α-helix in Pfr, reflected by the negative signal at *ca.* 1655 cm^{-1}, to a β-hairpin/β-sheet structure in Pr, as indicated by two bands at *ca.* 1630 and 1640 cm^{-1}. The assignment of these bands to the secondary structure transition of the tongue has been discussed in detail previously.[11,15,22,24,33,52] Note that the subtraction procedure may overemphasize subtle structural differences of the peptide segments in the Pr (or Pfr) states of the three phytochromes. As a consequence, the difference signals may exhibit slightly different positions and amplitudes although they reflect the same gross structural changes.

Chromophore–protein interactions with the carbonyl groups of rings A and D

The region of the C=O stretching modes, however, displays quite remarkable differences between the three phytochromes. We have therefore compared this region with the RR spectra of Pr and Pfr which offer the advantage of providing absolute signals although the signal-to-noise (S/N) ratio is relatively low. Furthermore, the RR spectra allows distinguishing between signals from the C=O stretching of the chromophore and the protein as the latter are not resonance enhanced. In this way, we have previously analyzed in detail the C=O stretching modes of Agp1, taking into account also calculated and further experimental data of isotopically labelled compounds.[13,32,53] Thus, two C=O stretching modes of ring D were identified in both Pfr and Pr that differ with respect to the extent of hydrogen bonding interactions (Fig. 6B–D). This finding is related to the structural heterogeneity of ring D that is also reflected by the two C–D methine bridge HOOP modes (see Fig. 2). In contrast, only one ring A C=O stretching mode was found at 1726 and 1730 cm^{-1} in Pfr and Pr, respectively. Also for Agp2 an assignment of the C=O stretching modes has been suggested previously but without considering RR spectra,[22] now shown in Fig. 6D. The RR data confirm the previous assignments with one exception. The positive band at 1733 cm^{-1} (Pr) was previously attributed to the C=O stretching of a yet not identified protonated Asp or Glu.[22] In view of the observation of this band in the RR spectra it must be largely due to a chromophore mode, although an additional contribution from an Asp or Glu cannot be ruled out rigorously. Hence, the band at 1733 cm^{-1} is assigned to the ring A C=O stretching in analogy to Agp1. Its counterpart in Pfr is observed at a very similar frequency (1730 cm^{-1}). The close proximity of these two bands accounts for the lack of a pronounced signal in the IR difference spectrum. A second band at 1718 cm^{-1} (1697 cm^{-1}) in Pr (Pfr) has been unambiguously assigned to a C=O

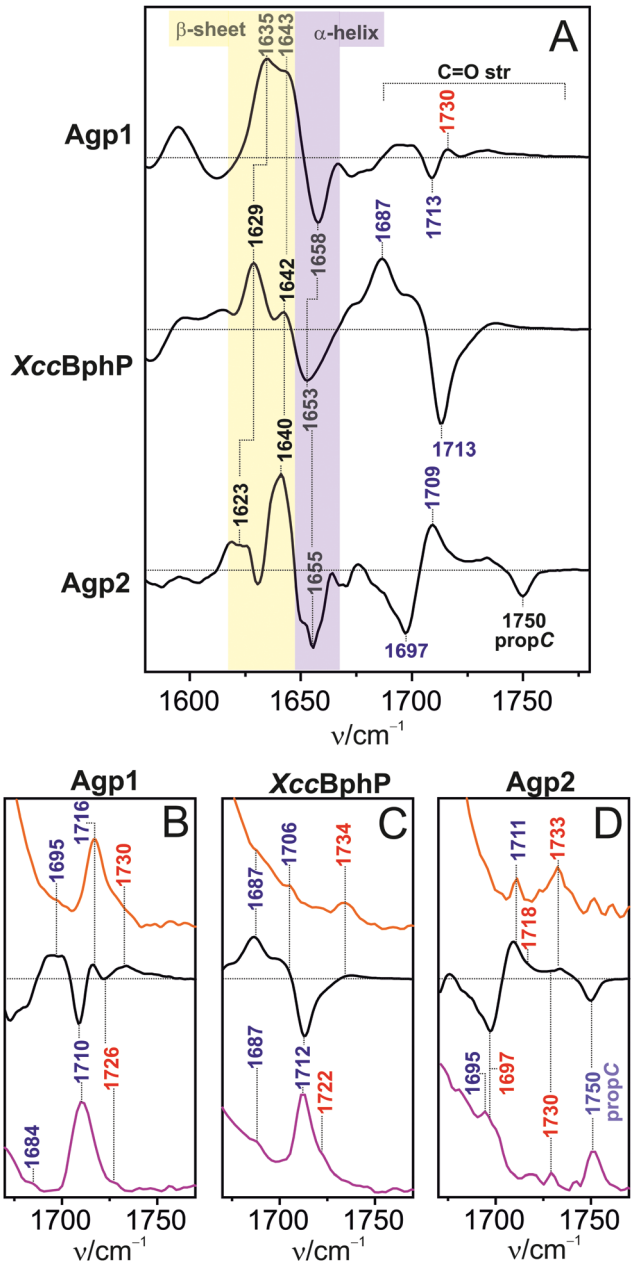

Fig. 6 (A) IR difference spectra "Pr minus Pfr" of Agp1, *Xcc*BphP, and Agp2, obtained at 20 °C. The positive and negative peaks refer to peaks from the Pr and Pfr state, respectively. The yellow- and violet-shaded signals highlight the amide I bands due to the α-helical and β-sheet segments. The region of the C=O stretching modes of the chromophore and amino acid side chains is further compared with the RR spectra of Pr (orange traces) and Pfr (magenta traces) in B, C, and D. The blue and red peak labels correspond to the C=O stretching modes of the pyrrole rings D and A, respectively.

stretching of ring A as well,[22] implying that in Agp2 ring A displays a significant heterogeneity in terms of hydrogen bonding interactions. For the corresponding ring D mode, the present RR and IR results consistently reveal only one mode for Pr and Pfr at *ca.* 1711 and 1695 cm^{-1}, in line with the previous analysis.[22] In terms of the C=O stretching modes of rings A and D, *Xcc*BphP is more closely related to Agp1 rather than to Agp2, since it displays as well bands of two C=O stretching modes of ring D and one C=O stretching of ring A both in Pr and Pfr at positions similar to the corresponding modes in Agp1. In addition to the carbonyl stretching modes of ring A and D, we note the band at 1750 cm^{-1} in Pfr of Agp2. This band is not observed in Pr implying a deprotonation of prop*C* with the formation of Pr. No band close to this position was found for Agp1 and *Xcc*BphP, neither in Pfr nor in Pr.

Discussion

We presented a spectroscopic analysis of the structural changes of three phytochromes during their phototransformation. The results are now discussed in terms of common and distinct structural and mechanistic properties that have specific functional impact (Table 2).

Structural differences in the parent states

We start the discussion with Agp1 and Agp2 as representatives of bathy and prototypical phytochromes. First, in Agp1 we identified a considerable structural heterogeneity, which is reflected by the C–D methine bridge HOOP modes. In addition, we also noted two bands due to ring D C=O stretching modes, implying that there are at least two sub-states differing with respect to subtle structural details of ring D and the adjacent methine bridge, *i.e.* the isomerization site. In contrast, there is no indication for any structural heterogeneity of the isomerization site (ring D) in Agp2.

Agp2 shows an unusually slow H/D exchange at ring D that requires several days to be completed at ambient temperature, in contrast to the instantaneous exchange at the other rings.[22,23] Presumably, the slow exchange kinetics reflects the strong electrostatic binding of the carboxylate side chain of Asp196 (Agp2) with the ring D N–H group that keeps it in the position of the *ZZEssa* configuration of Pfr. Hence, the slow H/D exchange at ring D corresponds to a slow thermal Pfr → Pr conversion. In fact, such a slow H/D exchange was not observed for phytochromes exhibiting a measurable thermal Pfr → Pr conversion such as Agp1 (Table 2).

In general, thermal reversion between the parent states requires the transient formation of an enol tautomer of the BV as postulated by Lagarias and Rapoport,[46] and recently confirmed by identification of an enol tautomer in the Pr state of Agp2.[22] However, the reactivity of the enol tautomer depends on the electron density distribution in the C–D methine bridge which in turn is controlled by the hydrogen bonding and electrostatic environment of ring D.[52] Thus, not in each case, the relative enol contribution is proportional to the rate of thermal double bond isomerization.[22,52] Nevertheless, so far the Pr state of Agp2 is the only state for which an enol form has been detected spectroscopically. This keto-enol tautomerism together with the ring D structural heterogeneity and the stability of the Asp196-ring D salt bridge in the Pfr state are key structural parameters that control the kinetics of the

thermal reactions between Pr and Pfr. In each phytochrome, reaction routes in both directions exist due to the principle of microscopic reversibility. The ratio of the corresponding rate constants, *i.e.*, the equilibrium constant of the parent states in the dark, thus reflects how specific structural parameters lower or raise the energy barriers in either direction (Table 2). In this way, it can readily be rationalized that Pr and Pfr are the most stable states in Agp1 and Agp2, respectively. *Xcc*BphP displays structural properties of both representatives (Table 2). In this sense, its classification as a bathy-like phytochrome is somewhat arbitrary. Therefore, it is not surprising that in *Xcc*BphP both parent states coexist in the dark, albeit with a preference for the Pfr state specifically in the full-length protein. This preference can be altered by modifying one of these critical structural parameters listed in Table 2. For instance, replacing Asp199 by a non-polar amino acid (Ala) prevents formation of Pfr whereas Asn and Gln, *i.e.* amino acids with hydrogen bonding capacity, shift the thermal equilibrium towards Pr,[54,55] due to the lack of the Pfr-stabilizing salt bridge with the ring D N–H group. Also, substitutions in the tongue region may affect the relative stabilization of Pr and Pfr. In the *Xcc*BphP variants W478A and S474E, the Pr/Pfr equilibrium is shifted towards the Pr state, presumably due to the destabilization of the Pfr state either by removing the π–π interactions between His194 and Trp478 in W478A or by repulsive effects of Glu474 with Asp199 in S474E.[56]

Whereas the structural heterogeneity of ring D may lower the barrier for the thermal isomerization of the chromophore, a structure-function relationship is not immediately evident for the structural heterogeneity of the A–B methine bridge in all three phytochromes and the ring A carbonyl group in Agp2, evidenced by the twofold appearance of the respective A–B and C=O stretching modes (Table 1). This heterogeneity is not restricted to the parent states which may reflect parallel photoconversion pathways.[9]

Reaction sequences of the phototransformations

To analyze the photoinduced processes of the three phytochromes by RR spectroscopy, we varied the trapping temperature from −160 °C to room temperature. The RR spectra obtained in this way were disentangled to yield a minimum number of different component spectra that allows for a satisfactory simulation of the experimental data.[9] Thus, one selects those intermediates that differ with respect to structural and electronic properties of the chromophore. This criterion also holds for detection with UV-vis spectroscopy, on the basis of which the present reaction scheme was derived nearly forty years ago.[57] In fact, the RR results for all three phytochromes studied in this work can be rationalized in terms of this sequence of intermediates, which is also an appropriate description for the photoinduced processes at ambient temperature.[8,58–60] However, each of these intermediates may comprise several conformational sub-states, in analogy to the concept introduced by Frauenfelder and coworkers.[61] These sub-states differ in small structural details, and their thermal decays are associated with low energy barriers of different heights depending on the specific protein environment. Accordingly, cryogenic trapping may cause the accumulation of different (sub-)states in the various phytochromes which in turn may account for small differences between the conjugate spectra. For instance, the Meta-F spectra (Fig. 3) display the N–H ip mode of rings B and C at 1560 (Agp1), 1563 (*Xcc*BphP), and 1553 cm^{-1} (Agp2). These differences may reflect the reorganization of the hydrogen-bonding network that seems to occur in discrete steps (sub-states) during the lifetime of Meta-F.[15,24] In the same way, one could rationalize other small spectral differences in the Meta-F state (*e.g.*, the position of the C–D stretching mode) as well as in other intermediates. One particularly striking example for the role of the energy landscape is the fact that it was not possible to identify a Lumi-R intermediate of *Xcc*BphP. Evidently, the energy barrier for its decay to Meta-Ra is too low to accumulate a sufficiently high contribution of a Lumi-R at any temperature.[9] Furthermore, specific sub-states may evade detection also because of a low spectral distinctness with respect to other states. For instance, temperature-dependent X-ray crystallography of the bathy phytochrome *Pa*BphP (*P. aeruginosa*) identified stepwise chromophore structural changes in Lumi-F-like intermediate, starting at the isomerization site (rotation of the C–D methine bridge) and followed by structural alterations also of the B–C and A–B methine bridges to form a ''late'' Lumi-F state.[62] The latter two structural changes are difficult to detect due to the intrinsically weak RR activity of the corresponding stretching modes and their overlap with the dominant C–D stretching. Thus, in Agp2 only one Lumi-F state could be identified by RR spectroscopy. Altogether, we therefore conclude that all three phytochromes run through the same Pr → Pfr and Pfr → Pr photoconversion routes including the same intermediate states with very similar structural properties. There is only one notable exception, which refers to the protonation state of prop*C* during the Pfr → Pr photoconversion (*vide infra*).

Proton transfer reactions during the photoconversions

In all three phytochromes studied here we have identified proton transfer steps that are associated with the phototransformations (Table 2). Most remarkable is the Pr → Pfr conversion which in Agp1 was found to be coupled with the deprotonation of a N–H group of the chromophore (ring B or ring C) in the Meta-Rc state, followed by the transient transfer of a proton to solution phase.[21,41,47] Re-uptake of a proton and re-protonation of the tetrapyrrole occurs with the decay of Meta-Rc and the formation of Pfr. Interestingly, a Meta-Rc with a deprotonated chromophore was also identified in Agp2 and *Xcc*BphP. Only the location of the deprotonation site in Meta-Rc, *i.e.* ring B or ring C, is different and presumably depends on the local electrostatics. These findings suggest that the proton transfer processes associated with the formation and decay of Meta-Rc are a general mechanistic property of all phytochromes. In fact, a transient proton release and re-uptake by the protein was also observed in cyanobacterial Cph1 from *Synechocystis* 6803,[20,41] and a Meta-Rc-type intermediate has

Table 1 Characteristic modes in the various states of Agp1, *Xcc*BphP, and Agp2[a]

		Protonated chromophore states					
Species	Mode	Pfr	Lumi-F	Meta-F	Pr	Lumi-R	Meta-Ra
Agp1	A–B	1620, 1611	1650, 1639	1646	1649, 1639	1621, 1629	1647
*Xcc*BphP		1607	nd	1649	1649	nd	1648, 1637
Agp2		nd	1608	1649	1649, 1642	1621	1637
Agp1	C–D	1600	1620	1627	1627	1596	1621
*Xcc*BphP		1594	1617	1624	1622	nd	1621
Agp2		1600	1608	1619	1622	1609	1605
Agp1	Ring D	nd	1625	nd	nd	1598	nd
*Xcc*BphP		nd	1617	nd	nd	nd	nd
Agp2		nd	1622	nd	nd	nd	nd
Agp1	B–C	nd	1600	1596	1600	nd	1593
*Xcc*BphP		nd	1585	1585	1600	nd	1593
Agp2		1578	1583	1585	nd	1582	1586
Agp1	C═O A	1726			1730		
*Xcc*BphP		1722			1734		
Agp2		1697, 1730			1718, 1733		
Agp1	C═O D	1684, 1710			1695, 1716		
*Xcc*BphP		1687, 1712			1687, 1706		
Agp2		1695			1711		
Agp1	N–H ip	1551	1569, 1551	1560	1571	1564	1570
*Xcc*BphP		1550	1551	1563	1571	nd	1565
Agp2		1549	1552	1553	1571	1549	1565

		Meta-Rc	
		Ring B deprotonated	Ring C deprotonated
Agp1	Ring B		1591
*Xcc*BphP		1583	
Agp2		1597	
Agp1	Ring C		1602
*Xcc*BphP		1602	
Agp2		1615	

[a] Mode frequencies are expressed by cm^{-1}; modes of the protonated tetrapyrrole: A–B, B–C, and C–D: stretching modes of the respective methine bridges; ring D, C═C stretching mode of ring D and its vinyl substituent; N–H ip, in-plane bending mode of the N–H groups of rings B and C; C═O A and C═O D, C═O stretching modes of the ring A and D. Modes of the deprotonated chromophore: ring B, C═C stretching localized in ring and the adjacent (B–C) methine bridge; ring C, C═C stretching localized in ring and the adjacent (C–D) methine bridge. The assignments are discussed in the text; nd = not detected.

Table 2 Structural properties and their functional impact in bathy and prototypical phytochromes

			Observed in		
No.	Structural parameter	Functional impact	Agp2	*Xcc*BphP	Agp1
1	Ring D/C–D heterogeneity	Favors thermal Pfr → Pr transition	No	Yes	Yes
2	Slow H/D exchange ring D	Disfavors thermal Pfr → Pr transition	Yes[a]	Yes	No
3	Enol/keto equilibrium in Pr	Favors thermal Pr → Pfr transition	Yes[a]	No	No
4	Ring A/A–B heterogeneity	?	Yes	Yes	Yes
5	Protonated prop*C* in Pfr and deprotonation in Pr	Mechanism of tongue restructuring	Yes	No	No
6	deprotonated BV in Meta-Rc and reprotonation in Pfr	Mechanism of tongue restructuring	Yes	Yes	Yes

[a] Assuming that H/D exchange rate at ring D (half time *ca.* 450 h) corresponds to the rate-limiting step of the Pfr → Pr conversion in Agp2,[23] the combination with the spectroscopically determined half time for the Pr → Pfr conversion of *ca.* 30 s[24] yields a [Pfr]/[Pr] equilibrium constant of *ca.* 5×10^4.

been detected in eukaryotic and prokaryotic phytochromes studied so far.[9,13]

The situation is different for the Pfr → Pr conversion. This reaction sequence does not involve an intermediate with a deprotonated chromophore. However, in Agp2 proton transfer from the prop*C* to His278 occurs,[22,24] which appears to be a unique feature of bathy phytochromes.[23] The only exception may be the myxobacterial phytochrome *Sa*BphP2 from *Stigmatella aurantiaca* which also displays a protonated and deprotonated prop*C* in Pfr and Pr, respectively.[13] In contrast, no proton transfer steps were identified in the Pfr → Pr photoconversion of *Xcc*BphP and Agp1 as well as in any other prototypical phytochrome.

Interestingly, all proton transfer steps in both photoconversion routes occur prior to or concomitant with the secondary structure transition of the tongue during the transition from Meta-Rc → Pfr and Meta-F → Pr, which already suggests a coupling between both types of processes. In fact, for Agp2 and

genetically engineered variants it has been shown that the α-helix/β-sheet transformation of the tongue is required for the proton transfer from prop*C* to His278.[24] The displacement of the proton is associated with a significant change of the local electric field, which in turn was proposed to be functional for the secondary structure transition.[12,24] Since this mechanistic pattern seems to hold in general, a proton transfer might also take place with the decay of Meta-F in Agp1 and *Xcc*BphP although it was not visible in the present IR and RR spectroscopic experiments.

Conclusions

Agp1, Agp2, and *Xcc*BphP are considered as representatives of specific classes of phytochromes, *i.e.* prototypical, bathy, and bathy-like phytochromes. Nevertheless, the present RR and IR spectroscopic analysis together with previous spectroscopic and structural data demonstrate that in each case photoswitching follows essentially the same reaction sequence of states as inferred from the properties of the chromophore. Furthermore, all three phytochromes undergo restructuring of the tongue as the putative functionally crucial change of the photosensor structure. Differences between the three phytochromes can be grouped into two categories: first, the specific protein environment controls details of the chromophore structure and affects the barrier for the thermal decay reactions of the individual intermediate states; second, proton transfer processes that are tightly coupled to the structural transitions of the tongue proceed presumably *via* the same mechanism along the Pr → Pfr conversion route whereas the reverse Pfr → Pr photoconversion includes different pathways. These mechanistic differences, however, do not coincide with classification of phytochromes in prototypical and bathy (or bathy-like) phytochromes. Here, the distinction criterion is essentially the ratio between the thermal conversion rate between Pr and Pfr, which – as shown in this work – can be traced back to molecular structure parameters stabilizing or destabilizing the Pr or Pfr state.

Conflicts of interest

There are no conflicts to declare.

Acknowledgements

This work was supported by the Deutsche Forschungsgemeinschaft (DFG) through the CRC 1078 ''Protonation Dynamics in Protein Function'' (project B06 to P. H. and P. S, and C02 to M. A. M.). Further support was obtained from the Einstein Center of Catalysis EC^2 (to M. A. M., P. H. and P. S.).

References

1 N. C. Rockwell, Y.-S. Su and J. C. Lagarias, Phytochrome Structure and Signaling Mechanisms, *Annu. Rev. Plant Biol.*, 2006, **57**, 837–858.
2 H. Wang, Phytochrome signaling: Time to tighten up the loose ends, *Mol. Plant*, 2015, **8**, 540–551.
3 T. Lamparter, N. Krauß and P. Scheerer, Phytochromes from Agrobacterium fabrum, *Photochem. Photobiol.*, 2017, **93**, 642–655.
4 J. Hughes, Phytochrome cytoplasmic signaling, *Annu. Rev. Plant Biol.*, 2013, **64**, 377–402.
5 E. Sethe Burgie and R. D. Vierstra, Phytochromes: An Atomic Perspective on Photoactivation and Signaling, *Plant Cell*, 2014, **26**, 4568–4583.
6 G. Gourinchas, S. Etzl, C. Göbl, U. Vide, T. Madl and A. Winkler, Long-range allosteric signaling in red light–regulated diguanylyl cyclases, *Sci. Adv.*, 2017, **3**, 1–12.
7 G. Gourinchas, U. Heintz and A. Winkler, Asymmetric activation mechanism of a homodimeric red light-regulated photoreceptor, *eLife*, 2018, **7**, 1–25.
8 V. A. Sineshchekov, Photobiophysics and photobiochemistry of the heterogeneous phytochrome system, *Biochim. Biophys. Acta*, 1995, **1228**, 125–164.
9 F. Velazquez Escobar, C. Kneip, N. Michael, T. Hildebrandt, N. Tavraz, W. Gärtner, J. Hughes, T. Friedrich, P. Scheerer, M. A. Mroginski and P. Hildebrandt, The Lumi-R Intermediates of Prototypical Phytochromes, *J. Phys. Chem. B*, 2020, **124**, 4044–4055.
10 D. Buhrke, U. Kuhlmann, N. Michael and P. Hildebrandt, The Photoconversion of Phytochrome Includes an Unproductive Shunt Reaction Pathway, *ChemPhysChem*, 2018, **19**, 566–570.
11 G. Merga, M. Fernandez Lopez, P. Fischer, P. Piwowarski, Z. Nogacz, A. Kraskov, D. Buhrke, F. Velazquez Escobar, N. Michael, F. Síebert, P. Scheerer, F. Bartl and P. Hildebrandt, Light- and Temperature-dependent Dynamics of Chromophore and Protein Structural Changes in Bathy Phytochrome Agp2, *Phys. Chem. Chem. Phys.*, 2021, **19**, 18197–18205.
12 A. Kraskov, J. Von Sass, A. D. Nguyen, T. O. Hoang, D. Buhrke, S. Katz, N. Michael, J. Kozuch, I. Zebger, F. Siebert, P. Scheerer, M. A. Mroginski, N. Budisa and P. Hildebrandt, Local Electric Field Changes during the Photoconversion of the Bathy Phytochrome Agp2, *Biochemistry*, 2021, **60**, 2967–2977.
13 A. Kraskov, D. Buhrke, P. Scheerer, I. Shaef, J. C. Sanchez, M. Carrillo, M. Noda, D. Feliz, E. A. Stojković and P. Hildebrandt, On the Role of the Conserved Histidine at the Chromophore Isomerization Site in Phytochromes, *J. Phys. Chem. B*, 2021, **125**, 13696–13709.
14 S. Nagano, P. Scheerer, K. Zubow, N. Michael, K. Inomata, T. Lamparter and N. Krauß, The Crystal Structures of the N-terminal Photosensory Core Module of Agrobacterium Phytochrome Agp1 as Parallel and Anti-parallel Dimers, *J. Biol. Chem.*, 2016, **291**, 20674–20691.
15 A. Schmidt, L. Sauthof, M. Szczepek, M. F. Lopez, F. Velazquez Escobar, B. M. Qureshi, N. Michael, D. Buhrke, T. Stevens, D. Kwiatkowski, D. von Stetten, M. A. Mroginski, N. Krauß, T. Lamparter, P. Hildebrandt and P. Scheerer, Structural snapshot of a bacterial phytochrome in its functional intermediate state, *Nat. Commun.*, 2018, **9**, 1–13.

16 N. C. Rockwell and J. C. Lagarias, The Structure of Phytochrome: A Picture Is Worth a Thousand Spectra, *Plant Cell*, 2006, **18**, 4–14.
17 B. Karniol and R. D. Vierstra, The pair of bacteriophytochromes from Agrobacterium tumefaciens are histidine kinases with opposing photobiological properties, *Proc. Natl. Acad. Sci. U. S. A.*, 2003, **100**, 2807–2812.
18 J. Hughes, Phytochrome three-dimensional structures and functions, *Biochem. Soc. Trans.*, 2010, **38**, 710–716.
19 H. Takala, A. Björling, O. Berntsson, H. Lehtivuori, S. Niebling, M. Hoernke, I. Kosheleva, R. Henning, A. Menzel, J. A. Ihalainen and S. Westenhoff, Signal amplification and transduction in phytochrome photosensors, *Nature*, 2014, **509**, 245–248.
20 J. J. Van Thor, B. Borucki, W. Crielaard, H. Otto, T. Lamparter, J. Hughes, K. J. Hellingwerf and M. P. Heyn, Light-induced proton release and proton uptake reactions in the cyanobacterial phytochrome Cph1, *Biochemistry*, 2001, **40**, 11460–11471.
21 B. Borucki, D. von Stetten, S. Seibeck, T. Lamparter, N. Michael, M. A. Mroginski, H. Otto, D. H. Murgida, M. P. Heyn and P. Hildebrandt, Light-induced Proton Release of Phytochrome Is Coupled to the Transient Deprotonation of the Tetrapyrrole Chromophore, *J. Biol. Chem.*, 2005, **280**, 34358–34364.
22 F. Velazquez Escobar, P. Piwowarski, J. Salewski, N. Michael, M. Fernandez Lopez, A. Rupp, M. B. Qureshi, P. Scheerer, F. Bartl, N. Frankenberg-Dinkel, F. Siebert, M. A. Mroginski and P. Hildebrandt, A protonation-coupled feedback mechanism controls the signalling process in bathy phytochromes, *Nat. Chem.*, 2015, **7**, 423–430.
23 F. Velázquez Escobar, D. Buhrke, N. Michael, L. Sauthof, S. Wilkening, N. N. Tavraz, J. Salewski, N. Frankenberg-Dinkel, M. A. Mroginski, P. Scheerer, T. Friedrich, F. Siebert and P. Hildebrandt, Common Structural Elements in the Chromophore Binding Pocket of the Pfr State of Bathy Phytochromes, *Photochem. Photobiol.*, 2017, **93**, 724–732.
24 A. Kraskov, A. D. Nguyen, J. Goerling, D. Buhrke, F. Velazquez Escobar, M. Fernandez Lopez, N. Michael, L. Sauthof, A. Schmidt, P. Piwowarski, Y. Yang, T. Stensitzki, S. Adam, F. Bartl, I. Schapiro, K. Heyne, F. Siebert, P. Scheerer, M. A. Mroginski and P. Hildebrandt, Intramolecular Proton Transfer Controls Protein Structural Changes in Phytochrome, *Biochemistry*, 2020, **59**, 1023–1037.
25 S. P.-A. Fodor, J. Clark Lagarias and R. A. Mathies, Resonance Raman analysis of the Pr and Pfr forms of phytochrome, *Biochemistry*, 1990, **29**, 11141–11146.
26 F. Andel, J. C. Lagarias and R. A. Mathias, Resonance Raman analysis of chromophore structure in the lumi-R photoproduct of phytochrome, *Biochemistry*, 1996, **35**, 15997–16008.
27 J. Dasgupta, R. R. Frontiera, K. C. Taylor, J. C. Lagarias and R. A. Mathies, Ultrafast excited-state isomerization in phytochrome revealed by femtosecond stimulated Raman spectroscopy, *Proc. Natl. Acad. Sci. U. S. A.*, 2009, **106**, 1784–1789.
28 Y. Mizutani, S. Tokutomi and T. Kitagawa, Resonance Raman spectra of the intermediates in phototransformation of large phytochrome: Deprotonation of the chromophore in the bleached intermediate, *Biochemistry*, 1994, **33**, 153–158.
29 J. Matysik, P. Hildebrandt, W. Schlamann, S. E. Braslavsky and K. Schaffner, Fourier-Transform Resonance Raman Spectroscopy of Intermediates of the Phytochrome Photocycle, *Biochemistry*, 1995, **34**, 10497–10507.
30 C. Kneip, P. Hildebrandt, W. Schlamann, S. E. Braslavsky, F. Mark and K. Schaffner, Protonation state and structural changes of the tetrapyrrole chromophore during the Pr → Pfr phototransformation of phytochrome: A resonance Raman spectroscopic study, *Biochemistry*, 1999, **38**, 15185–15192.
31 F. Siebert, R. Grimm, W. Rüdiger, G. Schmidt and H. Scheer, Infrared spectroscopy of phytochrome and model pigments, *Eur. J. Biochem.*, 1990, **194**, 921–928.
32 H. Foerstendorf, C. Benda, W. Gärtner, M. Storf, H. Scheer and F. Siebert, FTIR Studies of Phytochrome Photoreactions Reveal the C=O Bands of the Chromophore: Consequences for Its Protonation States, Conformation, and Protein Interaction, *Biochemistry*, 2001, **40**, 14952–14959.
33 E. A. Stojković, K. C. Toh, M. T.-A. Alexandre, M. Baclayon, K. Moffat and J. T.-M. Kennis, FTIR spectroscopy revealing light-dependent refolding of the conserved tongue region of bacteriophytochrome, *J. Phys. Chem. Lett.*, 2014, **5**, 2512–2515.
34 J. A. Ihalainen, E. Gustavsson, L. Schroeder, S. Donnini, H. Lehtivuori, L. Isaksson, C. Thöing, V. Modi, O. Berntsson, B. Stucki-Buchli, A. Liukkonen, H. Häkkänen, E. Kalenius, S. Westenhoff and T. Kottke, Chromophore-Protein Interplay during the Phytochrome Photocycle Revealed by Step-Scan FTIR Spectroscopy, *J. Am. Chem. Soc.*, 2018, **140**, 12396–12404.
35 U. Choudry, D. J. Heyes, S. J.-O. Hardman, M. Sakuma, I. V. Sazanovich, J. Woodhouse, E. De La Mora, M. N. Pedersen, M. Wulff, M. Weik, G. Schirò and N. S. Scrutton, Photochemical Mechanism of an Atypical Algal Phytochrome, *ChemBioChem*, 2018, **19**, 1036–1043.
36 L. H. Otero, F. A. Goldbaum, M. Fernández López, J. Rinaldi, F. Velázquez-Escobar, H. R. Bonomi, S. Klinke, P. Hildebrandt, M. A. Mroginski, A. A. Vojnov and F. Malamud, Structure of the Full-Length Bacteriophytochrome from the Plant Pathogen Xanthomonas campestris Provides Clues to its Long-Range Signaling Mechanism, *J. Mol. Biol.*, 2016, **428**, 3702–3720.
37 J. G. Vicente and E. B. Holub, Xanthomonas campestris pv. Campestris (cause of black rot of crucifers) in the genomic era is still a worldwide threat to brassica crops, *Mol. Plant Pathol.*, 2013, **14**, 2–18.
38 H. R. Bonomi, L. Toum, G. Sycz, R. Sieira, A. M. Toscani, G. E. Gudesblat, F. C. Leskow, F. A. Goldbaum, A. A. Vojnov and F. Malamud, Xanthomonas campestris attenuates virulence by sensing light through a bacteriophytochrome photoreceptor, *EMBO Rep.*, 2016, **17**, 1565–1577.
39 S. Klinke, L. H. Otero, J. Rinaldi, S. Sosa, B. G. Guimarães, W. E. Shepard, F. A. Goldbaum and H. R. Bonomi, Crystallization and preliminary X-ray characterization of the full-length bacteriophytochrome from the plant pathogen *Xanthomonas campestris* pv. *campestris*, *Acta Crystallogr. Sect. F Struct. Biol. Commun.*, 2014, **70**, 1636–1639.

40 J. Salewski, F. V. Escobar, S. Kaminski, D. Von Stetten, A. Keidel, Y. Rippers, N. Michael, P. Scheerer, P. Piwowarski, F. Bartl, N. Frankenberg-Dinkel, S. Ringsdorf, W. Gaïtner, T. Lamparter, M. A. Mroginski and P. Hildebrandt, Structure of the biliverdin cofactor in the Pfr state of bathy and prototypical phytochromes, *J. Biol. Chem.*, 2013, **288**, 16800–16814.
41 F. Velazquez Escobar, C. Lang, A. Takiden, C. Schneider, J. Balke, J. Hughes, U. Alexiev, P. Hildebrandt and M. A. Mroginski, Protonation-dependent structural heterogeneity in the chromophore binding site of cyanobacterial phytochrome cph1, *J. Phys. Chem. B*, 2017, **121**, 47–57.
42 A. Takiden, F. Velazquez-Escobar, J. Dragelj, A. L. Woelke, E.-W. Knapp, P. Piwowarski, F. Bartl, P. Hildebrandt and M. A. Mroginski, Structural and Vibrational Characterization of the Chromophore Binding Site of Bacterial Phytochrome Agp1, *Photochem. Photobiol.*, 2017, **93**, 713–723.
43 F. Velazquez Escobar, T. Hildebrandt, T. Utesch, F. J. Schmitt, I. Seuffert, N. Michael, C. Schulz, M. A. Mroginski, T. Friedrich and P. Hildebrandt, Structural Parameters Controlling the Fluorescence Properties of Phytochromes, *Biochemistry*, 2013, **53**, 20–29.
44 P. Schwinté, H. Foerstendorf, Z. Hussain, W. Gärtner, M. A. Mroginski, P. Hildebrandt and F. Siebert, FTIR study of the photoinduced processes of plant phytochrome phya using isotope-labeled bilins and density functional theory calculations, *Biophys. J.*, 2008, **95**, 1256–1267.
45 M. A. Mroginski, F. Mark, W. Thiel and P. Hildebrandt, Quantum mechanics/molecular mechanics calculation of the Raman spectra of the phycocyanobilin chromophore in α-C-phycocyanin, *Biophys. J.*, 2007, **93**, 1885–1894.
46 J. C. Lagarias and H. Rapoport, Chromopeptides from Phytochrome. The Structure and Linkage of the PR Form of the Phytochrome Chromophore, *J. Am. Chem. Soc.*, 1980, **102**, 4821–4828.
47 D. Von Stetten, S. Seibeck, N. Michael, P. Scheerer, M. A. Mroginski, D. H. Murgida, N. Krauss, M. P. Heyn, P. Hildebrandt, B. Borucki and T. Lamparter, Highly conserved residues Asp-197 and His-250 in Agp1 phytochrome control the proton affinity of the chromophore and Pfr formation, *J. Biol. Chem.*, 2007, **282**, 2116–2123.
48 K. Smit, J. Matysik, P. Hildebrandt and F. Mark, Vibrational analysis of biliverdin dimethyl ester, *J. Phys. Chem.*, 1993, **97**, 11887–11900.
49 J. Matysik, P. Hildebrandt, K. Smit, A. Korkin, F. Mark, W. Gärtner, S. E. Braslavsky, K. Schaffner and B. Schrader, Vibrational Analysis of Biliverdin IXα Dimethyl Ester Conformers, *J. Mol. Struct.*, 1995, **348**, 225–228.
50 J. Matysik, P. Hildebrandt, K. Smit, F. Mark, W. Gärtner, S. E. Braslavsky, K. Schaffner and B. Schrader, Raman spectroscopic analysis of isomers of biliverdin dimethyl ester, *J. Pharm. Biomed. Anal.*, 1997, **15**, 1319–1324.
51 S. Osoegawa, R. Miyoshi, K. Watanabe, Y. Hirose, T. Fujisawa, M. Ikeuchi and M. Unno, Identification of the Deprotonated Pyrrole Nitrogen of the Bilin-Based Photoreceptor by Raman Spectroscopy with an Advanced Computational Analysis, *J. Phys. Chem. B*, 2019, **123**, 3242–3247.
52 M. Fernandez Lopez, A. D. Nguyen, F. Velazquez Escobar, R. González, N. Michael, Ż. Nogacz, P. Piwowarski, F. Bartl, F. Siebert, I. Heise, P. Scheerer, W. Gärtner, M. A. Mroginski and P. Hildebrandt, Role of the Propionic Side Chains for the Photoconversion of Bacterial Phytochromes, *Biochemistry*, 2019, **58**, 3504–3519.
53 N. Lenngren, P. Edlund, H. Häkkänen, H. Takala, B. Stucki-Buchli, J. Rumfeldt, I. Peshev, S. Westenhoff and J. A. Ihalainen, Coordination of the biliverdin D-ring in bacteriophytochromes, *Phys. Chem. Chem. Phys.*, 2018, **20**, 18216–18225.
54 V. Conforte, L. H. Otero, L. Toum, S. Sirigu, G. T. Antelo, J. Rinaldi, S. Foscaldi, S. Klinke, L. M.-G. Chavas, A. A. Vojnov, F. A. Goldbaum, F. Malamud and H. R. Bonomi, Pr-favoured variants of the bacteriophytochrome from the plant pathogen Xanthomonas campestris hint on light regulation of virulence-associated mechanisms, *FEBS J.*, 2021, 1–17.
55 G. T. Antelo, M. Sánchez-Lamas, F. A. Goldbaum, L. H. Otero, H. R. Bonomi and J. Rinaldi, A Spectroscopy-based Methodology for Rapid Screening and Characterization of Phytochrome Photochemistry in Search of Pfr-favored Variants, *Photochem. Photobiol.*, 2020, **96**, 1221–1232.
56 L. H. Otero, S. Foscaldi, G. T. Antelo, G. L. Rosano, S. Sirigu, S. Klinke, L. A. Defelipe, M. Sánchez-Lamas, G. Battocchio, V. Conforte, A. A. Vojnov, L. M.-G. Chavas, F. A. Goldbaum, M.-A. Mroginski, J. Rinaldi and H. R. Bonomi, Structural basis for the Pr-Pfr long-range signaling mechanism of a full-length bacterial phytochrome at the atomic level, *Sci. Adv.*, 2021, **7**, 1097.
57 P. Eilfeld and W. Rüdiger, Absorption spectra of phytochrome intermediates, *Zeitschrift fur Naturforsch. - Sect. C J. Biosci.*, 1985, **40**, 109–114.
58 A. R. Holzwarth, J. Wendler, B. P. Ruzsicska, S. E. Braslavsky and K. Schaffner, Picosecond time-resolved and stationary fluorescence of oat phytochrome highly enriched in the native 124 kDa protein, *Biochim. Biophys. Acta, Protein Struct. Mol. Enzymol.*, 1984, **791**, 265–273.
59 A. R. Holzwarth, E. Venuti, S. E. Braslavsky and K. Schaffner, The phototransformation process in phytochrome. I. Ultrafast fluorescence component and kinetic models for the initial Pr → Pfr transformation steps in native phytochrome, *Biochim. Biophys. Acta, Bioenerg.*, 1992, **1140**, 59–68.
60 P. Schmidt, T. Gensch, A. Remberg, W. Gärtner, S. E. Braslavsky and K. Schaffner, The complexity of the Pr to Pfr phototransformation kinetics is an intrinsic property of native phytochrome, *Photochem. Photobiol.*, 1998, **68**, 754–761.
61 H. Frauenfelder, B. H. Mcmahon, R. H. Austin, K. Chu and J. T. Groves, The role of structure, energy landscape, dynamics, and allostery in the enzymatic function of myoglobin, *Proc. Natl. Acad. Sci. U. S. A.*, 2001, **98**, 2370–2374.
62 X. Yang, Z. Ren, J. Kuk and K. Moffat, Temperature-scan cryocrystallography reveals reaction intermediates in bacteriophytochrome, *Nature*, 2011, **479**, 428–431.

